

# Sensor-Driven Online Coverage Planning for Autonomous Underwater Vehicles

Liam Paull, Sajad Saeedi, Mae Seto and Howard Li

**Abstract**—At present, autonomous underwater vehicle (AUV) mine countermeasure (MCM) surveys are normally pre-planned by operators using ladder or zig-zag paths. Such surveys are conducted with side-looking sonar sensors whose performance is dependant on environmental, target, sensor, and AUV platform parameters. It is difficult to obtain precise knowledge of all of these parameters to be able to design optimal mission plans offline.

This research represents the first known sensor driven online approach to seabed coverage for MCM. A method is presented where paths are planned using a multi-objective optimization. Information theory is combined with a new concept coined branch entropy based on a hexagonal cell decomposition. The result is a planning algorithm that not only produces shorter paths than conventional means, but is also capable of accounting for environmental factors detected *in situ*. Hardware-in-the-loop simulations and in water trials conducted on the IVER2 AUV show the effectiveness of the proposed method.

**Index Terms**—autonomous underwater vehicles, coverage path planning, information gain, hardware-in-the-loop, mine countermeasure, sidescan sonar, adaptive mission planning

## I. INTRODUCTION

Sensor-driven path planning refers to a strategy for gathering sensor measurements that support a sensing objective. When sensors are installed on robotic platforms, an objective could be to plan the platform's path based on sensor readings to achieve a specific goal. Various approaches have been proposed for planning the paths of mobile robots with on-board sensors to enable navigation and obstacle avoidance in unstructured dynamic environments. These methods are not directly applicable to robotic sensors whose primary goal is to support a sensing objective, rather than to navigate a dynamic environment as part of a goal. Traditional mission planning methods focus on how sensor measurements best support the robot mission, rather than robot missions that best support the sensing objective. In the case of area coverage for mine countermeasures (MCM), the sensing objective defines the mission and therefore must be treated with adequate priority.

Autonomous underwater systems technology is lagging behind ground and aerial robotics systems. The main reasons are the rapid attenuation of high-frequency signals, and the

costly and challenging development environment. These obstacles must be overcome as the US Navy has referred to underwater mine removal as the most problematic mission facing unmanned undersea vehicles and the Navy at large [1]. Defining efficient paths for AUVs performing area coverage for MCM is particularly challenging because the sonar sensor performance can vary greatly depending on factors which in general cannot be perfectly predicted before the start of the mission.

In this research, we propose an online approach to autonomously achieve underwater seabed coverage for MCM. Sensor objectives for the coverage task are particularly hard to define because of the uncertainty of sensor measurements so information gain is exploited as a goodness criterion [2]. However, it is shown that the information gain method alone is not sufficient to achieve global goals when there is incomplete prior knowledge about the environment. To compensate, the concept of branch entropy is proposed. Although the proposed research can be applied to diverse missions or sensors, it is particularly well-suited to AUV MCM missions where the seabed is scanned using a side-looking sensor (SLS).

Prior to this work, few if any research proposed online strategies to underwater area coverage. Usually AUVs are pre-programmed with waypoints that specify a structured path, such as a zig-zag or lawn mower [3]. In this case, performance will rely heavily on the accuracy of information about the workspace and vehicle localization. In the approach taken here, path planning is achieved through reconciling behaviors that represent the multiple objectives defined for efficient mission completion as the vehicle navigates through the workspace. The proposed approach has the advantages that:

- 1) The total paths and times required to cover a workspace are shorter in many cases.
- 2) There is no need for pre-programmed waypoints.
- 3) The AUV will maintain heading for better data mosaicing in the presence of currents or erratic waypoint tracking behavior caused by poor navigation or controller performance.
- 4) It is adaptive to any changes in environmental conditions that can be detected *in situ*.
- 5) It is able to generate paths for complex and non-convex environment shapes such as would typically found in harbours.
- 6) Preference is given to viewing seabed from different insonification angles, which is beneficial for target recognition [4].

The performance of the approach is evaluated via hardware-in-the-loop (HWIL) simulation and implementation on the IVER2 AUVs developed by OceanServer Inc.

The remainder of the paper is organized as follows: Section

Liam Paull is a COBRA team member with the Department of Electrical and Computer Engineering, University of New Brunswick, Fredericton, Canada, liam.paull@unb.ca

Sajad Saeedi G. is a COBRA team member with the Department of Electrical and Computer Engineering, University of New Brunswick, Fredericton, Canada, sajad.saeedi.g@unb.ca

Mae Seto is with Defence Research and Development Canada, Halifax, Nova Scotia, Canada, Mae.Seto@drdc-rddc.gc.ca

Howard Li is a COBRA team member with the Department of Electrical and Computer Engineering, University of New Brunswick, Fredericton, Canada, howard@unb.ca

II will provide background and literature review. Section III describes the proposed solutions, including the information gain and branch entropy behaviors, Section IV describes the experimental setup and the HWIL simulation framework. Section V shows simulation and experimental results, while a more in-depth discussion is performed in Section VI. Section VII makes general conclusions and discusses potential future work.

## II. BACKGROUND OF RESEARCH

This section will review previous results in the areas of AUV path planning and path planning for coverage as well as discuss the operation of the sidescan sonar sensor. For a tutorial on basic robotics motion planning, the reader is referred to [5].

### A. AUV path planning

Traditionally, the task of path planning has been to find a curve in the configuration space,  $C$  that connects a start location to an end location in some ‘optimal’ way.

Significant research has been done on start point to goal point path planning for AUVs. In most cases, an optimal path is found by some metric subject to holonomic or other constraints.

For example, one of the first known papers to discuss path planning of AUVs was published by Warren in 1990 [6]. Potential fields are used to avoid obstacles and local minima are avoided by considering the global path. In [7] an optimal kinematic control scheme is proposed where the cost function to be minimized is the integral of a quadratic function of the velocity components. A mixed integer linear programming method has also been used in [8] to find paths for adaptive sampling that maximize the line integral of the uncertainty of sensor readings along the proposed path. This type of algorithm is used as an alternative to static buoys for collecting oceanic data such as temperature and salinity. The approach taken is somewhat similar to the path planning algorithm proposed here, except that the metric for benefit in the objective function is a maximum sum of probabilities and paths planned are greedy. Information has been used for AUV path planning, for example [9] uses mutual information as the benefit metric in the objective function, combined with a recursive greedy planner. However, the proposed grid decomposition results in very constricted paths.

### B. Path planning for coverage

In the coverage task, instead of navigating to a goal the objective now becomes to pass a sensor or end effector over every point in a workspace.

As described in Choset’s survey of complete coverage methods [10], there are heuristic, random, and cell decomposition techniques. A heuristic defines a set of rules to follow that will result in the entire environment being covered. For example, in [11], complete coverage is achieved based on sensing critical points [11], and in [12], a method of building corridors is used based on maximizing some quality function. A key

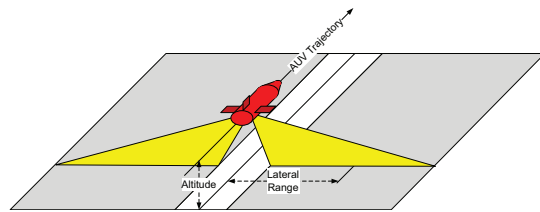


Fig. 1. An example of the AUV trajectory and corresponding area covered by its SSS.

facet of these approaches is having obstacles to be able to generate the rules. Cell decomposition is used to divide up the environment into a manageable number of cells or areas that can be searched like a graph or tree. Once all cells have been covered, then the entire workspace has been covered. Decomposition can be approximate [2], semi-approximate, or exact [10].

These approaches have been applied to AUV coverage path planning in various forms. For example, in [13] a coverage algorithm for MCM with a SLS is proposed that uses cell decomposition and exploits the limiting assumption that mines are normally placed in lines.

The term Boustrophedon search is used in ground robotics to describe a path that follows a simple back and forth motion [14]. In [15], a Boustrophedon decomposition is combined with the Generalized Voronoi Diagram to derive paths for coverage of a highly unstructured or non-convex environment. However, this algorithm presumes that absolute knowledge of the environment is known *a priori* and all planning is done offline. The Boustrophedon search is often referred to as the lawn mower pattern in AUV survey planning, and will be used as a method of comparison in this work.

If it is assumed that the AUV will follow parallel tracks then the location of these tracks can be further optimized using a process as described in [16]. The metric for optimality is maximizing the mean probability of detection over the workspace. The dependence of probability of detection on seabed type and range is described. While the proposed method is very useful, the planned paths are constricted to parallel tracks and planning is done offline.

### C. Sidescan Sonar Sensor

Many underwater MCM missions are conducted with a side-looking sensor: either a synthetic aperture sonar (SAS) or a sidescan sonar sensor (SSS). In this research the SSS has been used. The SSS uses the returns from emitted high frequency sound to generate an image of the seabed. An object sitting on the seabed will cast a sonar shadow that can be analyzed to determine if the shape is suggestive of a mine. The onboard SSS gathers data as the AUV moves forward in rectilinear motion and leaves a narrow channel of unscanned seabed directly beneath it. An AUV path and corresponding SSS coverage swath are shown in Fig. 1. SSS returns are combined with onboard navigation data to provide geo-referenced mosaics of the seabed (Fig. 2). When the sonar makes sharp turns, areas on the outside of the turn are missed completely due to the finite ping rate of the sonar, and areas on the inside of the turn can become completely distorted. In both

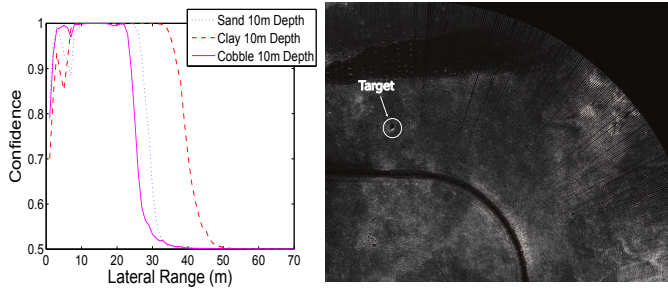


Fig. 2.  $\mathcal{P}(y)$  curves for three different seabed conditions (left) and sample geo-referenced SSS data (right)

cases, it becomes very difficult for automatic target recognition (ATR) systems that rely on template matching to identify targets in these areas [17]. The angle of incidence of the sonar beam with the seabed has a significant effect on the size of the shadow cast by an object and therefore the probability of successful mine detection and classification. The Extensible Performance and Evaluation Suite for Sonar (ESPRESSO) is a tool developed by the NATO Undersea Research Centre to evaluate the sonar performance characteristics for a specific set of environmental conditions [18]. The program generates a  $\mathcal{P}(y)$  lateral range curve that indicates the probability that a target at a specified lateral range from a sonar’s track will be detected. Parameter values that affect the generation of the  $\mathcal{P}(y)$  curve are described in Table I along with the general way in which these parameters are determined.

Category	Parameters	Method of Detection
Environmental, $E$	Seabed type	Sonar or camera imagery
	Water salinity and temperature	CT sensor
	Water clarity	Camera
	Water depth	Sonar
Target, $F$	Mine type, size and configuration	Only available through prior surveys of the area
Sonar, $S$	Frequency and range of sensor	Known beforehand from sensor specifications
Vehicle $V$	AUV speed	Doppler velocity log (DVL)
	AUV depth	Pressure sensor
	Navigational error	Output from inertial navigation system

TABLE I  
PARAMETERS AFFECTING SONAR PERFORMANCE CHARACTERISTICS

Fig. 2 shows the  $\mathcal{P}(y)$  curves generated by ESPRESSO for three different seabed types: cobble, sand, and clay, all at a depth of 10 m. The meaning of “confidence” on the y-axis will be formally defined in Section III.

It should be explicitly stated that the purpose of this work is not to verify the ESPRESSO model, but rather to plan paths based on the model. Any underwater sonar sensor’s performance will be affected by some or all of the parameters described in Table I and it cannot be assumed in general that all of these parameters are known beforehand. In this work we evaluate the benefit of potential actions using the ESPRESSO model to represent the sensor characteristic but without assuming known parameters.

### III. PROPOSED METHODS

The backbone of the proposed approach is an objective function that is evaluated over the domain of all possible desired headings:  $\psi_d = \{0..360\}$ . The general form of the function is given by:

$$R(\psi_d) = w_B B(\psi_d) + w_G G(\psi_d) + w_J J(\psi_d), \quad (1)$$

where  $R$  is the total utility,  $B$  is the information gain,  $G$  is the branch entropy,  $J$  is the benefit of maintaining the current heading, and  $w_B$ ,  $w_G$ , and  $w_J$  are the respective weights. All functions will be explicitly defined, but, in general, the function  $B(\psi_d)$  prioritizes headings that cover the most area in the short term, the function  $G(\psi_d)$  prioritizes over headings that will help the agent complete its coverage mission in the longer term, and the function  $J(\psi_d)$  prioritizes over headings closest to the current heading so that obtained SSS data is valid. The functions  $B$  and  $G$  will be described in detail in Section III-A and III-B respectively.

It should be noted that this desired heading is used as a reference to an inner loop controller that produces the desired control plane values. As such, it is reasonable to evaluate (1) over a domain of angles that includes sharp turns. There is no violation of dynamic constraints since these will be imposed in the inner loop.

The optimization takes place over heading reference only and it is assumed that desired speed and depth are generated by some other method. In this case speed and altitude reference are held constant and tracked by inner loop PID controllers. The reference depth can be calculated from the reference altitude using known bathymetry or data from onboard sensors.

Tuning of the weights is an important consideration. In the present implementation, trial and error has been used to tune the weights, however, it would be simple to optimize them with some meta heuristic method such as genetic algorithms or particle swarm optimization.

The evaluation of the multi-objective function is done using Interval Programming (IvP) through the MOOS-IvP framework [19], [20]. Each term in the objective function is defined as a behavior which generates a piecewise linear objective function at each iteration of the outer-loop controller. Accuracy of the underlying objective functions can be traded off against computation time by specifying the number of pieces in the piecewise linear approximation. As a result, the domain is discretized. However, the discretization does not need to be consistent over all objective functions and also need not be uniform.

Each objective function is scaled such that the maximum utility is 100. As a result, the units of the individual functions can be disregarded.

#### A. The Information Gain Behavior

Information theory will be used to quantify utility over the short term to define the function  $B$  from 1.

The mutual information, or expected entropy reduction (EER):

$$\bar{I}(X, Z) = H(X) - \bar{H}(X|Z), \quad (2)$$

defines a scalar quantity that represents the *a priori* expected amount of information about state  $X$  contained in observation  $Z$ . To evaluate  $\bar{H}(X|Z)$  we take the expectation over the measurement  $Z$ :

$$\begin{aligned} \bar{H}(X|Z) &= E_z\{H(X|Z)\} \\ &= - \int P(Z) \int P(X|Z) \log P(X|Z) dx dz. \end{aligned} \quad (3)$$

$P(Z)$  is the probability of obtaining measurement  $Z$ .

The essential aspect of this definition is that it specifies a way of combining the potential benefits of sensor measurements *additively*. Consider some control action at time  $t$  to be  $U_t$ . If the ratio of the control frequency to the sensor frequency is  $n$  then each control action  $U_t$  will result in a set of  $n$  independent measurements  $\{Z_1, Z_2, \dots, Z_n\}$ . The total expected *information gain* of  $U_t$  can be expressed as:

$$B(U_t) = \sum_{k=1}^n \bar{I}(X, Z_k). \quad (4)$$

To define the information gain objective function, information gained must be formulated as a function of desired heading  $\psi_d$ . This is achieved by defining a track starting at the AUVs current location,  $(x, y)$ , and traveling a fixed distance,  $r$ , at every potential heading  $\psi_d$ . The measurements that will be made can be predicted and then (4) can be used to evaluate the expected information gained from traveling along the given track.

Define the variable  $M_{ij} \in \{0, 1\}$  to represent the actual presence of a target at the point  $(i, j)$  in the discretized workspace,  $W$ . Then, consider the variable  $m_{ij} \in \{0, 1\}$  to be our belief about the presence of a mine at location  $(i, j)$ . The confidence at location  $(i, j)$ , denoted by  $c_{ij}$ , represents the confidence that if a mine exists it will be detected. Therefore, we can define a binary RV  $T_{ij}$  such that:

$$\begin{aligned} P(T_{ij} = 1) &= P(m_{ij} = M_{ij}) = c_{ij} \\ P(T_{ij} = 0) &= P(m_{ij} \neq M_{ij}) = 1 - c_{ij} \end{aligned} \quad (5)$$

Then the entropy of  $T_{ij}$  can be represented as:

$$H(T_{ij}) = -c_{ij} \log(c_{ij}) - (1 - c_{ij}) \log(1 - c_{ij}) \quad (6)$$

From (6) it follows that

$$\lim_{c_{ij} \rightarrow 1} H(T_{ij}) = 0. \quad (7)$$

This implies that maximizing the confidence over the environment minimizes the entropy of  $T_{ij}$  for all  $i, j$ . As a result, the information gain objective function can be defined in terms of gaining information about  $T_{ij}$ .

1) *The probability of mine detection:* From the above formulation it is possible to derive the probability that a mine actually exists given that we detected one at location  $(i, j)$ . If the number of mines in a given area  $A$  can be known or estimated as  $N$ , then the probability that a mine exists at any given location  $(i, j)$ , denoted  $p^{ij}$  can be approximated by:

$$p^{ij} \approx \frac{N}{A}, \quad (8)$$

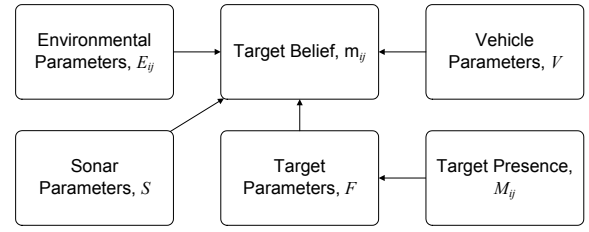


Fig. 3. Bayesian network representing target detection. Arrows represent conditional probabilities.

then, from Bayes' formula

$$P(M_{ij} = 1 | m_{ij} = 1) = \frac{c_{ij} p^{ij}}{2c_{ij} p^{ij} - c_{ij} - p^{ij} + 1} \quad (9)$$

defines the probability that a mine actually is present given that we think one is present. This relation can be used to validate the assumptions used in this paper such as the validity of the sensor models and the target recognition systems.

Let the proposed path to be evaluated be represented by  $\mathcal{C}$ . The path begins at the AUV's current location,  $(x, y)$  and moves a distance  $r$  at heading  $\psi_d$ :

$$\begin{aligned} \mathcal{C} : [0, 1] &\rightarrow \mathcal{C}_{free}, s \rightarrow \mathcal{C}(s) \\ \mathcal{C}(0) &= (x, y) \\ \mathcal{C}(1) &= (x + r \cos(\psi_d), y + r \sin(\psi_d)) \end{aligned} \quad (10)$$

Let the proposed action,  $U_t$  from (4) be defined as exactly following the proposed track. Since  $r$ ,  $x$ , and  $y$  are assumed constant, the information gain resulting from following the proposed track can be defined as a function of the desired heading,  $\psi_d$ . It should be noted that these tracks could not be followed in reality due to dynamic constraints of the robotics platform. However, this framework can be used to evaluate the expected benefit of potential desired headings and as such removes the horizon constraint of information gain approaches that operate over actual control actions such as [21]. These desired headings are used as a reference input to an inner loop controller that defines the control plane values. The confidence over the environment is updated based on the actual heading, not the desired heading. As a result, the actual trajectory will be smoother with less variations in actual heading.

Based on the parameters affecting sonar performance given in Table I, target detection can be expressed as the Bayesian network [2] given in Fig. 3.

We can express the joint probability as:

$$\begin{aligned} P(m_{ij}, E_{ij}, S, F, V, M_{ij}) &= \\ P(m_{ij} | E_{ij}, S, F, V) P(F | M_{ij}) P(E_{ij}) P(S) P(V) P(M_{ij}) \end{aligned} \quad (11)$$

However, since we are only interested in estimating the confidence over the workspace and not the actual presence of mines, (5) can be used to rewrite the right hand side of (11) as:

$$P(T_{ij} | E_{ij}, S, F, V) P(E_{ij}) P(S) P(F) P(V). \quad (12)$$

Define  $Z_k^{ij} = \{E_{ij}, S, F, V\}$  as the set of all parameters at time  $k$ . Then we can further simplify (12) to

$P(T_{ij}|Z_k^{ij})P(Z_k^{ij})$  where it is assumed that environmental, sensor, target, and vehicle parameters are independent. The probability  $P(T_{ij}|Z_k^{ij})$  is given by a  $\mathcal{P}(y)$  curve generated with the ESPRESSO model where  $y$  is the orthogonal distance of location  $(i, j)$  from the AUV track.  $P(Z_k^{ij})$  is the probability that we are using the correct  $\mathcal{P}(y)$  curve to evaluate the confidence at location  $(i, j)$ . In this case, we do not assume perfect information about the parameters that are contained within  $Z_k^{ij}$ , however we can use (3) to define the expected entropy of  $T_{ij}$  conditional on the measurement represented by  $Z_k^{ij}$  as:

$$\begin{aligned} \bar{H}(T_{ij}|Z_k^{ij}) &= E_{z_k} \{H(T_{ij}|Z_k^{ij})\} \\ &= - \sum_{Z_k^{ij}} P(Z_k^{ij}) [-c_{ij}^k \log c_{ij}^k \\ &\quad - (1 - c_{ij}^k) \log (1 - c_{ij}^k)] \end{aligned} \quad (13)$$

where  $c_{ij}^k$  is the confidence at location  $(i, j)$  after measurement  $Z_k^{ij}$ .

If there is no knowledge of environmental conditions beforehand, the distribution of  $Z$  can be initialized as uniform across all possible parameter values. As the AUV traverses the workspace, some unknown parameters can be measured *in situ* using sensors as described in Table I. Once these measurements are made in the field, the distribution of  $Z$  used for calculating the expected entropy using (13) can be updated for the rest of the mission.

The new confidence determined from  $P(T_{ij}|Z_k^{ij})$  should be combined with the existing confidence at  $(i, j)$ ,  $c_{ij}$  using the process described in Sec. III-C, to produce the new confidence at that location  $c_{ij}^k$ .

The EER at location  $(i, j)$  caused by measurement  $Z_k$  then follows from (2) as:

$$\bar{I}(T_{ij}, Z_k^{ij}) = H(T_{ij}) - \bar{H}(T_{ij}|Z_k^{ij}) \quad (14)$$

Define the line that is perpendicular to  $\mathcal{C}$  and aligns with SSS reading  $Z_k$  as  $\mathcal{C}^\perp$ . The EER over the entire workspace,  $W$ , brought about by a measurement  $Z_k$  is then the sum of the EER along the line  $\mathcal{C}^\perp$ .

$$\bar{I}(W, Z_k) = \sum_{(i,j) \text{ on } \mathcal{C}^\perp} \bar{I}(T_{ij}, Z_k^{ij}) \quad (15)$$

Given that there is no overlap between subsequent sonar pings from a SSS, the total expected information gain brought about by moving along the path  $\mathcal{C}$  can be expressed as:

$$B(\psi_d) = \sum_{k=1}^n \bar{I}(W, Z_k) \quad (16)$$

where  $n$  is the number of sensor observations.

As the  $\mathcal{P}(y)$  curve does not have a closed form representation, gradient-based optimizations are not possible. For this reason, IvP is suitable.

It should also be noted that the seabed environment that is being sensed is assumed static. As a result, information is never lost only gained by sensing the environment.

An AUV is shown in an environment in Fig. 8. The IvP functions at the stop time are shown in Fig. 9. Note that

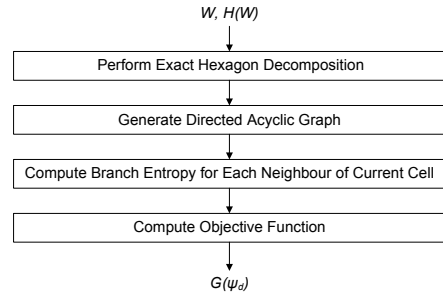


Fig. 4. Flow diagram depicting the generation of the branch entropy objective function.

the highest utility for the information gain objective function in this case is approximately  $90^\circ$ , the direction that is being traveled, and the lowest utility is the reverse direction,  $270^\circ$ , because almost no new information would be gained from moving over the path that was just traveled.

## B. Branch Entropy

In this section, the  $G(\psi_d)$  term of the objective function (1) will be motivated and derived.

1) *Motivation:* The information gain method has been shown to be effective for solving the path planning problem when *a priori* knowledge of the environment, obstacles, and targets is available [2]. However, the approach taken here removes this requirement. In the sensor-driven approach, the information gain  $B$  is useful for evaluating the benefits of each of the potential next moves, but when complete coverage is the goal, this approach reduces to a greedy-first search (GFS).

It is necessary to include a parameter in the objective function that helps the AUV achieve its global goal. The benefits of including the branch entropy (BE) in the objective function are:

- It helps the AUV finish sections before it leaves them.
- It allows the AUV to find the areas of the workspace that are not covered.
- It acts as a tie-breaker so the AUV does not enter infinite loops and converges to complete coverage.

2) *Overview of Approach:* A block diagram showing an overview of the proposed approach is shown in Fig. 4. The inputs are the workspace,  $W$ , and the entropies over the entire workspace,  $H(W)$ . The output is the BE objective function,  $G(\psi_d)$ .

The workspace is decomposed into equal sized hexagon cells. The average entropy of the cells is used to determine which areas of the environment are not covered. A formula is derived whereby each neighbour of the cell currently occupied by the AUV is given a value representing the benefit of heading towards that particular cell. The value is determined by how much entropy there is down that branch of the directed acyclic graph, with priority given to high entropy areas that are nearby. The result is that, by simply applying a formula on the decomposition and without performing an exhaustive search, the AUV can determine what areas of the map are left to be explored.

Each of the blocks in Fig. 4 will be described in detail in the subsequent sections.

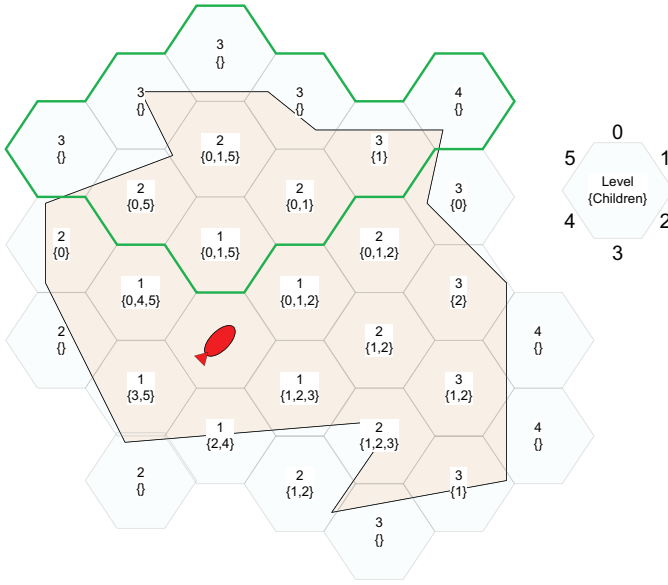


Fig. 5. A workspace with a hexagon cell decomposition. The cells that will be in branch 0 have been outlined.

3) *Exact Hexagon Decomposition*: Cell decomposition is an effective way to reduce the path planning problem into the searching of a tree [14]. Normally, the cells are either exactly or approximately decomposed into rectangloids (i.e. a grid decomposition), although other polygonal shapes have been proposed [22]. However, these decompositions assume that once the robot moves into a cell, that it is efficiently covered. This assumption is not applicable to the the SSS geometry so a new decomposition method is proposed. A main benefit of the hexagon decomposition is that the distance from the center of any cell to the center of any adjacent cell is the same.

A hexagon decomposition is performed such that the union of all cells,  $C_k, k = 1..N$  covers the entire workspace:

$$W \subseteq \bigcup_{k=1}^N C_k. \quad (17)$$

Associated with each cell is an average entropy,  $\hat{H}_k$ , which represents a measure of the average uncertainty over the area of the workspace that falls within that cell:

$$\hat{H}_k = \frac{1}{\eta} \sum_{(i,j) \in C_k \cap W} H(T_{ij}), \quad (18)$$

where  $\eta$  is the number of grid cells in hexagon cell  $C_k$ . Each cell is also assigned a level,  $l$ , which is the minimum number of cells that must be traversed to reach the presently occupied cell  $C_p$ , and a list of children, which are all neighbours in level  $l + 1$ .

A hexagon decomposition of a workspace is shown in Fig. 5. The workspace is the shaded area underneath the hexagons. The hexagon on the right shows the numbering convention for the neighbours. The cells in branch 0 are indicated by the bold outline.

4) *The Directed Acyclic Graph*: The directed acyclic graph (DAG) uses the levels and children of each cell to build an alternate data structure. Every cell  $C_i$  appears only once in the graph, and is at level  $l$ . There can be several paths from

$C_p$  to  $C_i$  but they must all be the same minimum length. The hexagon decomposition geometry is exploited such that every cell at level  $l$  is the same distance from the current cell.

Each neighbour of  $C_p$  becomes a child in the graph. The neighbours of those nodes become children provided they are not already in the graph at higher a level. This process continues until all cells are in the DAG.

Algorithm 1 details the process of building the DAG. The inputs are  $C_p$ , the current cell, and  $C$ , the set of all other cells.

---

**Algorithm 1** Build\_DAG( $C, C_p$ )

---

```

DoneList  $\leftarrow$   $C_p$ 
level  $\leftarrow$  1
while DoneList  $\neq$  C do
  level  $\leftarrow$  level + 1
  for  $n \leftarrow$  Each node in level - 1 do
    CurrentList  $\leftarrow$   $\emptyset$ 
    n.children  $\leftarrow$   $\emptyset$ 
    for  $k \leftarrow$  All neighbours of n do
      if  $k \notin$  DoneList then
        n.children  $\leftarrow$  n.children  $\cup$  k
        k.value  $\leftarrow$   $C_k$ .entropy
        if  $k \notin$  CurrentList then
          CurrentList  $\leftarrow$  CurrentList  $\cup$  k
        end if
      end if
    end for
  DoneList  $\leftarrow$  DoneList  $\cup$  CurrentList
end while

```

---

5) *Derivation of Branch Entropy*: The BE is used to evaluate how much entropy there is down each branch of the DAG in order that preference will be given to the move that takes the AUV towards an unfinished area of  $W$ . Also, priority will be given to moves that have more unfinished area nearer to the current position so that the AUV does not leave an area before it is finished.

There will be a value of BE for each neighbour of the current cell  $C_p$  as each neighbour has its own branch in the DAG. In order for the BE to provide the benefits desired, cells that are at higher levels in the graph must be given more weight. For each neighbour,  $k = 0..5$ , of  $C_p$ , the BE,  $g_k$ , for a DAG with a total of  $L$  levels is given by:

$$g_k = \frac{\sum_{l=2}^L (L-l+1) \frac{\sum_{i=1}^{m_{lk}} \hat{H}_i}{m_{lk}}}{\sum_{l=1}^{L-1} l}. \quad (19)$$

where  $m_{lk}$  is the number of nodes in level  $l$  of branch  $k$ . In (19), the closer cells are weighted higher using an inverse linear function. Other weighting functions, such as exponential decay could have been used, and would produce similar results.

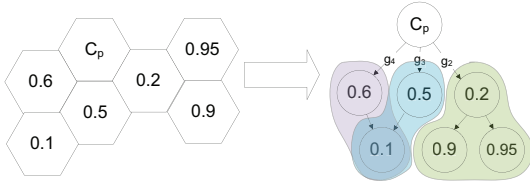


Fig. 6. A transformation from cell to DAG. (numbers in cells/nodes represent average cell entropy)

6) *Simple Example*: Fig. 6 shows the transformation from hexagon cells to DAG. The cell labeled  $C_p$  is the cell that the AUV is currently in, and the values in all of the other cells represent their average entropies. The corresponding BE for each of the three neighbours are calculated as:

$$\begin{aligned} g_4 &= 1/3((2)(0.6) + (1)(0.1)) = 0.433, \\ g_3 &= 1/3((2)(0.5) + (1)(0.1)) = 0.367, \\ g_2 &= 1/3((2)(0.2) + (1)(1/2)(0.95 + 0.90)) = 0.442. \end{aligned}$$

In this case  $g_2$  is the highest.

7) *Building the Branch Entropy Objective Function*: The values of branch entropy are treated as samples of the underlying objective function and are connected linearly to generate the full objective function. The 6 desired headings,  $\psi_d$  of known utility are  $60k^\circ, k = 0..5$ , which corresponds to the headings that pass through the midpoints of the neighbouring hexagon faces. The corresponding points used to generate the objective function for  $G(\psi_d)$  are  $(60k, g_k), k = 0..5$ . The known points are then connected with straight lines based on the piecewise linear framework of IvP. A general equation for the objective function,  $G(\psi_d)$  is derived that parameterizes each of the connecting lines:

$$G(\psi_d) = \frac{1}{60}(g_k - g_{k+1})\psi_d + g_k(1 - k) + g_{k+1}. \quad (20)$$

where

$$k = \lfloor \frac{\psi_d}{60} \rfloor. \quad (21)$$

Note that for consistency define  $g_6 = g_0$ .

An AUV is shown in an environment in Fig. 8. The IvP functions at the stop time are shown in Fig. 9. The branch entropy behavior is maximum at  $0^\circ$  and  $180^\circ$  as these headings point to the areas of the map that have unfinished areas.

### C. Combining Measurements From Different Insonification Angles

Automatic or manual target identification is greatly improved if the object of interest can be viewed multiple times from different angles of insonification [4], particularly in the case of non-symmetric targets as shown in Fig. 7, or rippled seabed types. As such, it is preferable to scan areas with non-parallel tracks. In other research, it has been assumed that measurements should be either dependent [16] or independent [23] regardless of insonification angle. Our approach accounts for the angles of insonification of the multiple views when combining subsequent observations of the same seabed location.

Let two confidences obtained from subsequent passes of location  $(i, j)$  be  $c_{ij}^1$  and  $c_{ij}^2$  with corresponding angles of

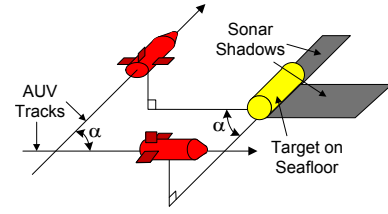


Fig. 7. Different views of asymmetric targets will provide different shadows. It is desirable for target recognition to view targets at different angles [4]

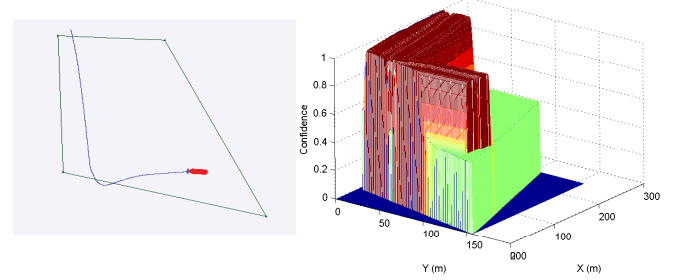


Fig. 8. A simulated path (left) with confidence map (right)

insonification  $\theta_1$  and  $\theta_2$ . Without loss of generality, we can assume that  $c_{ij}^1 \geq c_{ij}^2$ .  $\alpha$  is calculated as the acute angle of the intersection of two lines with directions  $\theta_1$  and  $\theta_2$  as shown in Fig. 7.

In the case that the two measurements are parallel, then  $\alpha = 0$  and the two confidences are considered to be dependant:

$$c_{ij}^{tot} = \max(c_{ij}^1, c_{ij}^2) = c_{ij}^1. \quad (22)$$

In the case that the two measurements are perpendicular, then  $\alpha = \pi/2$  and the two confidences are considered to be independent:

$$c_{ij}^{tot} = 1 - ((1 - c_{ij}^1)(1 - c_{ij}^2)). \quad (23)$$

If the angle  $0 < \alpha < \pi/2$  then it is assumed that the resulting confidence,  $c_{ij}^{tot}$  should be determined using:

$$c_{ij}^{tot} = \frac{2\alpha c_{ij}^2}{\pi}(1 - c_{ij}^1) + c_{ij}^1, \quad (24)$$

which describes a linear relation between dependence and independence based on the value of  $\alpha$ .

The conditional entropy defined in (13) therefore incorporates the angles of insonification in the computation of  $c_{ij}^k$ . As a result, the information gain objective function will preferentially select paths that result in views of the workspace from different aspects.

### D. The Collective Objective Function

According to (1), the final utility,  $R$ , is the weighted sum of the objective functions. In Fig. 9 the objective functions at a snapshot are shown together with the collective with  $w_B = 1.0$ ,  $w_G = 1.0$ , and  $w_J = 0.8$ . In this case, the collective objective function selects the heading at  $94^\circ$  to be the best desired heading.

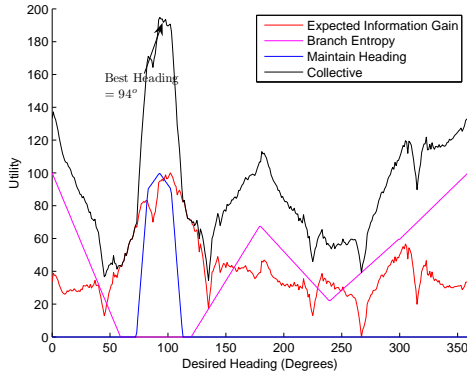


Fig. 9. The information gain, branch entropy, maintain heading, and collective objective functions corresponding to the path shown in Fig. 8

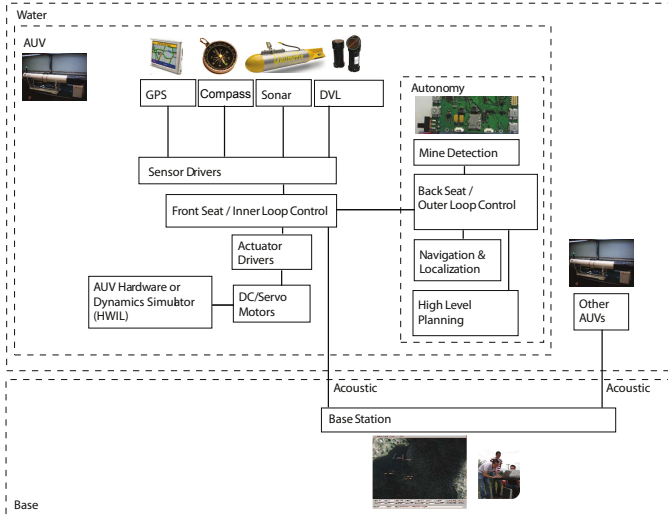


Fig. 10. System structure of the hardware-in-the-loop simulator

#### IV. EXPERIMENTAL SETUP

In order to test the control algorithms, a hardware-in-the-loop (HWIL) simulator with the Mission Oriented Operating Suite (MOOS) [20] is developed and shown in Fig. 10. A description of all hardware simulated components and real hardware is also given in Table. II. Also onboard the AUV but not simulated in the HWIL simulation was a Neil Brown CT sensor to gather water conductivity and temperature information.

The hardware implementation is done on the IVER2 AUV shown in Fig. 11. The IVER2's onboard computer (frontseat) contains navigation and inner loop control algorithms. These algorithms can be overwritten and raw sensor data can be fused using the *iOceanServerComms* application [25] which sends data to the backseat and commands to the frontseat using a serial connection. In the actual implementation, navigation and outer loop control were performed on the backseat using MOOS, while inner loop control remains on the frontseat.

Component	Hardware Simulation	Real Experiment
GPS Sensor	iGPS [24]	UBlox LEA-5H
Compass Sensor	iCompass [24]	OS5000-USG
Depth Sensor	iDepth [24]	MSI Depth sensor
Sonar Sensor	pConfidenceMap	Yellowfin Dual-Frequency 330/800 kHz Side-scan
DVL	iDVL [24]	SonTek/YSI DVL
Sensor Drivers	"iSensor" applications [24]	IVER2 frontseat
Inner Loop Control	pMarinePID [24]	IVER2 frontseat
Actuator Drivers	included in iActuation [24]	IVER2 frontseat
Actuator	iActuation [24]	130 Watt, 4000 RPM Brushless DC motor
Frontseat Computer	Dell Dual Core 3GHz	Intel 1.6 GHz ATOM processor
Frontseat - Backseat Communication	pMOOSBridge [24]	iOceanServerComms [25]
Backseat Computer	Dell Dual Core 3GHz	Intel 1.6 GHz ATOM processor
Outer Loop Control	IvP Helm [26]	IvP Helm [26]
Navigation and Localization	pEKF	pEKF
High Level Planning	Behaviors	Behaviors
Base Station	Dell Dual Core 3GHz	Windows Netbook
Backseat - Base Station Communication	pAcommsHandler & iModemSim [27]	WHOI $\mu$ Modem

TABLE II  
DESCRIPTION OF COMPONENTS USED FOR HWIL SIMULATION AND REAL HARDWARE TRIALS



Fig. 11. The path planned by the proposed planner for a for a square workspace with constant and *a priori* known parameters (left). The IVER2 AUV made by OceanServer Technology used for trials (right).

#### V. RESULTS

##### A. Simulation

The system is tested using the HWIL setup. The first simulation done is on a simple square environment with fixed and known environmental parameters. The resulting path is shown in Fig. 11.

As can be seen from the figure, the planner converges to a spiral-type path that efficiently covers the entire area. The spiral-type path is more efficient than the Boustrophedon or lawn mower path in this case because the AUV has to perform less turns and consequently will expend less energy. It is important to note that without any disturbance in parameters or oddly shaped environment that the planner does converge to a structured path.

Since in general the system is stochastic, a Monte Carlo style simulation is conducted to compare the performance for a developed random track algorithm, the information gain

behavior alone (IG), and information gain with branch entropy (IG/BE) by repeating the simulation 36 times with random initial conditions. The results are tested against the deterministic typical lawn mower pattern for a simple environment. Results for three different levels of desired confidence are shown in Table III, where  $\mu$  and  $\sigma$  correspond to the mean and the standard deviation of the 36 trials.

		Desired Confidence		
		.90	.95	.98
Search Method	Lawn Mower	1275	1545	2355
	Random	1279 [446]	1915 [460]	2299 [677]
	IG	1488 [362]	2429 [817]	3307 [730]
	IG/BE	1088 [105]	1458 [150]	1761 [160]

TABLE III

PERFORMANCE OF LAWN MOWER, RANDOM WALK, INFORMATION GAIN AND INFORMATION GAIN WITH BRANCH ENTROPY ALGORITHMS FOR DIFFERENT CONFIDENCE THRESHOLDS.

In the generation of the results in Table III, it is assumed that environmental and target parameters for the ESPRESSO model are unknown beforehand. As a result, the lawn mower tracks are based on the most pessimistic assumption of the unknown parameters. The lawn mower path length required to obtain 98% coverage is significantly higher because the tracks must be placed closely enough that the areas that are missed directly underneath the tracks are covered by subsequent tracks.

It is clear from the results that the information gain approach alone is not sufficient. The mean path lengths are considerably longer. Also note that the variances are also much larger, particularly for the 95% confidence case. This is characteristic of a greedy approach because sometimes it will get ‘lucky’ and find a good path very quickly, but when it is ‘unlucky’ it has a very difficult time completing the mission and the path length becomes very long.

It can also be challenging to design lawn mower paths in the case that the workspace is oddly shaped. For example consider Fig. 12. In this case parameters are considered fixed and known. For the case of low desired confidence thresholds, the lawn mower planner performs well. However, in the case that high confidence is desired, which is common, the lawn mower tracks must be designed so that the channel left by one track is covered by the next. Indeed this has been noted in the past as a shortcoming of the lawn mower method [3]. The IG/BE planner proposed produces a path with more path overlap, but less total sensor swath overlap allowing it to achieve high coverage faster than the lawn mower pattern. As the workspace shape becomes more irregular, the benefit of the proposed planner will increase.

In the case that the environmental parameters are known but vary over the workspace, the simplest way to construct the lawn mower path is to place tracks closely enough that coverage will be obtained even in the worst case over the environment. In Fig. 13 the parameters are assumed to be known beforehand where the seabed type varies between cobble, sand, and clay. The  $\mathcal{P}(y)$  curves for the three areas of the environment are shown in Fig. 2. In order to ensure coverage, the lawn mower tracks must be placed closely enough to guarantee coverage in the case that the seabed

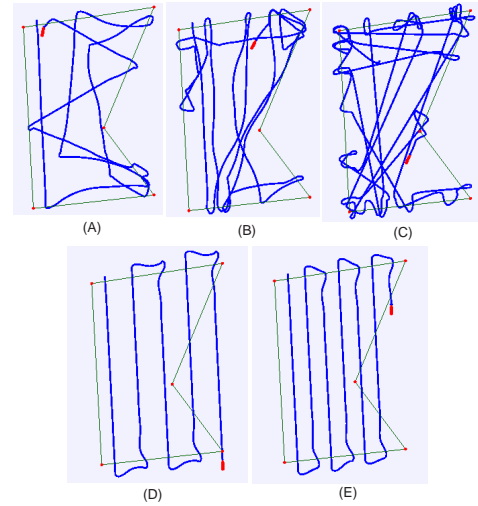


Fig. 12. A slightly more complex environment shape is simulated. Total area of environment is  $41250m^2$ . (a) Path planned by BE/IG planner for final confidence greater than 99%. Path length 1154.25m. (b) Path planned by IG planner alone for final confidence greater than 99%. Path length is 1639.34m. (c) Path planned by random track planner for final confidence greater than 99%. Path length is 1826.90m. (d) Deterministic lawn mower path for final confidence of 99%. Path length is 683.33m. (e) Deterministic lawn mower path for final confidence of 97%. Path length is 1221.64m. In order for the lawn mower path to obtain coverage greater than 97%, the valleys under the AUV track must be covered resulting in high sensor swath overlap between subsequent tracks in the lawn mower survey.

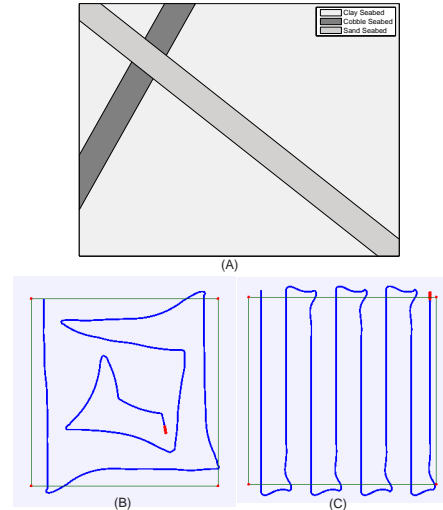


Fig. 13. (a) A 300m by 300m square workspace with variable parameters, in this case three different types of seabed, which are assumed to be known *a priori*. (b) The path planned by the proposed IG/BE planner. Path length to achieve 97% confidence is 1085.90. The AUV automatically devotes more time to the areas of seabed with poorer sensor performance (c) Deterministic path for a lawn mower pattern. Path length to achieve 97% is 1185.90. Note that if a higher coverage threshold was desired then the tracks would have to be significantly closer as described in Fig. 12.

is cobble, which is the worst case. The proposed IG/BE planner maintains the confidence map as the AUV traverses the workspace and is therefore better able to capitalize on the better sonar performance obtained in the case that the seabed type is clay.

The algorithm scales in constant time with the size of the workspace after an initialization since computations required for the information gain or branch entropy behaviors are all

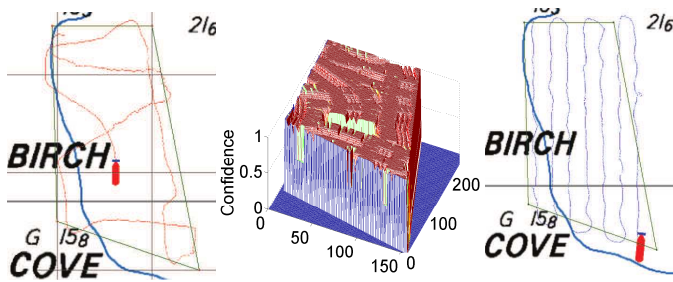


Fig. 14. Path taken by AUV in real trial (left), resulting confidence map (middle), and comparison lawn mower path (right).

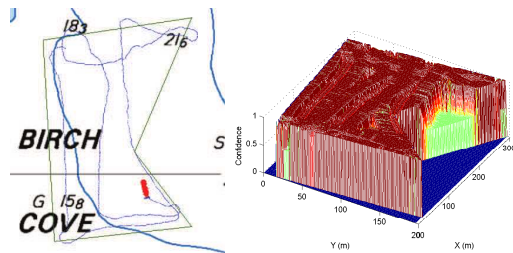


Fig. 15. Path taken by AUV in non-convex environment in real trial (left) and resulting confidence map (right)

done incrementally as the vehicle traverses the workspace.

### B. In-Water Trials

Tests were performed on OceanServer's IVER2 AUV in Aug. 2011 in Bedford Basin, Nova Scotia, Canada.

The AUV was able to successfully cover two environments within the limited operating region. A plot of a sample path taken in a simple convex environment and the corresponding final confidence map are shown in Fig. 14. The runs were stopped when confidence values reached 95%. A comparison lawn mower mission was also performed.

When comparing the two paths from Fig. 14, it is interesting to note that, although the desired tracks for the lawn mower are straight lines, the actual path oscillates across these desired paths. This is largely due to the inability of the frontseat controller to stabilize the heading in the presence of currents. It should be noted that the currents on the day when this trial was conducted (Sept. 1 2011) were extremely small, on the order of 0.2 knots at most. Because the proposed planner is designed to maintain headings, the outputted sonar data will be of higher quality thereby improving data mosaicing during post-processing and allowing targets to be identified more easily.

A more complex non-convex environment test was also conducted with results shown in Fig. 15. By comparison with Fig. 12, it is shown that the results from simulation and from water trials are very similar, confirming the validity of the simulations.

The path lengths for the trials are shown in Table IV.

## VI. DISCUSSION

As discussed, the status quo for AUV sidescan seabed surveys is to perform a structured search, either a lawn mower

	Path Length	Workspace Area
Proposed planner (Fig. 14)	1203 m	28 000 $m^2$
Lawn mower (Fig. 14)	1580 m	
Proposed planner (Fig. 15)	1661 m	41 250 $m^2$

TABLE IV  
SAMPLE PATH LENGTHS FOR PATHS PLANNED DURING HARDWARE TRIALS

or zig-zag type pattern. The waypoints that define the path are either input by a human operator or somehow optimized beforehand using a method such as [16]. The method proposed here is drastically different than this approach. The simulation and experimental results illustrate that the proposed planner is able to find shorter paths under many conditions. However, the benefits of the approach extend beyond simply shorter path lengths. In order to further compare the method presented against the standard lawn mower method, an empirical comparison is presented in Table V.

## VII. CONCLUSION AND FUTURE WORK

This research presents an online sensor-driven robotics path planner with particular application to seabed coverage with a sidescan sonar sensor and an autonomous underwater vehicle. The approach combines information theory with a new concept coined branch entropy to efficiently cover areas of seabed. Simulation results and real water trials illustrate the benefit of this approach over standard lawn mower planners. These advantages are: the total path length and time to cover an environment are shorter in many cases, heading is better maintained for data mosaicing, there is no need for predetermined waypoints, factors affecting sensor performance can be accounted for, the planner is able to autonomously handle very complex shaped environments, and the planner preferentially views the seabed from different insonification angles, which is preferable for target recognition.

In future work, the proposed approach will be extended to multiple searchers. This is particularly challenging given the difficult communication environment underwater. This will involve combining novel multi-AUV navigation techniques with a decentralized searching and planning approach. In addition, algorithms should be developed to optimize the selection of weights either statically or dynamically. Lastly, in order to increase the benefit of this algorithm to real-world applications, it is necessary to better formulate the ATR and sonar geo-referencing algorithms such that the confidence can be used to make accurate predictions of mine detection rates.

## ACKNOWLEDGEMENT

The authors would like to acknowledge the contributions of Vincent Myers, Warren Connors, and Jonathan Hudson at DRDC-Atlantic in addition to the anonymous reviewers who provided invaluable feedback. This research is supported by Natural Sciences and Engineering Research Council of Canada (NSERC), Defense R&D Canada - Atlantic, and New Brunswick Innovation Fund.

	Proposed Planner	Lawn Mower Approach
Coverage overlap	While it is acknowledged that there is some overlap as the path sometimes crosses itself, the actual amount of coverage overlap is reduced evidenced by the fact that coverage swaths can be more accurately estimated and accounted for online.	Guaranteeing high coverage requires tight spacing of lawn mower tracks which results in high coverage overlap, but in some cases when desired coverage is sufficiently low, overlap can be minimized.
Level of autonomy	Extremely high. One button solution.	Usually requires operator to specify waypoints to define tracks. In complex environments the performance is subject to the judgement and skill of the survey designer.
Total energy consumption	Fairly low since trajectories are smooth.	Requires sharp turns at the end of tracks and also high energy requirements to follow the track as shown by the jagged path in Fig. 14.
Online vs. offline	All planning takes place online. The main advantage as has been stated is that mission plans can be adaptive to environmental parameters and stochastic sensor measurements.	All planning is done offline. There is an inherent assumption with this type of planning that the vehicle trajectory will exactly follow the plan and that all environmental parameters will be as predicted.
Deterministic vs. stochastic	Stochastic in that it is capable of adapting to the stochastic nature of state estimation and sensor input.	Deterministic.
Completeness	Probabilistically complete - due to the BE behavior, the AUV is guaranteed to find the areas of the map that are not covered.	Although the motion plan can have a guarantee of completeness, there is no actual guarantee of that the entire workspace will be covered in reality.
Path tracking	Optimizes an objective function over heading so paths are not tracked.	Required to follow track between waypoints.
Level of feedback	Closed loop - sensor feedback used to update plan.	Open loop.
Computational requirements	High - requires simulation over headings for IG behavior but only a simple numerical calculation for the BE behavior.	Low.
Overall performance	Results in path with shorter path in general if environmental parameters are not known <i>a priori</i> and particularly in the case of complex environment geometries.	Paths tend to be longer if worst case environmental conditions are assumed. However, in ideal case with full prior knowledge, simple environment geometry and low required confidence threshold can provide better solution.

TABLE V  
COMPARISON OF PROPOSED METHOD AND STANDARD LAWN MOWER

## REFERENCES

- [1] U. Navy, "The navy unmanned undersea vehicle (UUV) master plan," U.S. Navy, Tech Rep. A847115, 2004.
- [2] C. Cai and S. Ferrari, "Information-driven sensor path planning by approximate cell decomposition," *IEEE Transactions on Systems, Man, and Cybernetics - Part B: Cybernetics*, vol. 39, no. 3, pp. 672–689, Jun. 2009.
- [3] B. Nguyen, D. Hopkin, and H. Yip, "Autonomous underwater vehicles a transformation of mine counter-measure operations," *Defense & Security Analysis*, vol. 24, no. 3, pp. 247–266, 2008.
- [4] J. Fawcett, V. Myers, D. Hopkin, A. Crawford, M. Couillard, and B. Zerr, "Multiaspect classification of sidescan sonar images: Four different approaches to fusing single-aspect information," *Oceanic Engineering, IEEE Journal of*, vol. 35, no. 4, pp. 863–876, Oct. 2010.
- [5] S. LaValle, "Motion planning," *Robotics Automation Magazine, IEEE*, vol. 18, no. 1, pp. 79–89, Mar. 2011.
- [6] C. Warren, "A technique for autonomous underwater vehicle route planning," *Oceanic Engineering, IEEE Journal of*, vol. 15, no. 3, pp. 199–204, Jul. 1990.
- [7] J. Biggs and W. Holderbaum, "Optimal kinematic control of an autonomous underwater vehicle," *Automatic Control, IEEE Transactions on*, vol. 54, no. 7, pp. 1623–1626, Jul. 2009.
- [8] N. Yilmaz, C. Evangelinos, P. Lermusiaux, and N. Patrikalakis, "Path planning of autonomous underwater vehicles for adaptive sampling using mixed integer linear programming," *Oceanic Engineering, IEEE Journal of*, vol. 33, no. 4, pp. 522–537, Oct. 2008.
- [9] J. Binney, A. Krause, and G. Sukhatme, "Informative path planning for an autonomous underwater vehicle," in *Robotics and Automation (ICRA), 2010 IEEE International Conference on*, May 2010, pp. 4791–4796.
- [10] H. Choset, "Coverage for robotics - a survey of recent results," *Annals of Mathematics and Artificial Intelligence*, vol. 31, pp. 113–126, 2001.
- [11] E. U. Acar and H. Choset, "Sensor-based coverage of unknown environments: Incremental construction of morse decompositions," *International Journal of Robotics Research*, vol. 21, pp. 345–367, 2002.
- [12] R. Wein, J. van den Berg, and D. Halperin, "Planning high-quality paths and corridors amidst obstacles," *The International Journal of Robotics Research*, vol. 27, pp. 1213–1231, 2008.
- [13] J. Stack and C. Smith, "Combining random and data-driven coverage planning for underwater mine detection," in *OCEANS 2003. Proceedings*, vol. 5, Sep. 2003, pp. 2463–2468.
- [14] H. Choset, "Coverage of known spaces: the boustrophedon cellular decomposition," *Autonomous Robots*, vol. 9, pp. 247–253, 2000.
- [15] C. Fang and S. Anstee, "Coverage path planning for harbour seabed surveys using an autonomous underwater vehicle," in *OCEANS 2010 IEEE - Sydney*, May 2010, pp. 1–8.
- [16] D. Williams, "On optimal AUV track-spacing for underwater mine detection," in *Robotics and Automation (ICRA), 2010 IEEE International Conference on*, May 2010, pp. 4755–4762.
- [17] P. Chapple, "Automated detection and classification in high-resolution sonar imagery for autonomous underwater vehicle operations," Maritime Operations Division DSTO Defence Science and Technology Organisation, DSTO-GD-0537, Dec. 2002.
- [18] G. Davies and E. Signell, "Espresso scientific user guide," NATO Underwater Research Centre, NURC-SP-2006-003, 2006.
- [19] M. Benjamin, J. Curcio, and P. Newman, "Navigation of unmanned marine vehicles in accordance with the rules of the road," in *Robotics and Automation, 2006. ICRA 2006. Proceedings 2006 IEEE International Conference on*, May 2006, pp. 3581–3587.
- [20] M. Benjamin, P. Newman, H. Schmidt, and J. Leonard, "An overview of MOOS-IvP and a brief users guide to the IvP Helm autonomy software," <http://dspace.mit.edu/bitstream/handle/1721.1/45569/MIT-CSAIL-TR-2009-028.pdf>, Jun. 2009.
- [21] J. Tisdale, Z. Kim, and J. Hedrick, "Autonomous uav path planning and estimation," *Robotics Automation Magazine, IEEE*, vol. 16, no. 2, pp. 35–42, Jun. 2009.
- [22] T. Oksanen and A. Visala, "Coverage path planning algorithms for agricultural field machines," *Journal of Field Robotics*, vol. 26, no. 8, pp. 651–668, Aug. 2009.
- [23] A. Rajala and D. Edwards, "Allocating AUVs for mine map development in MCM," in *OCEANS 2006 - Asia Pacific*, May 2006, pp. 1–8.
- [24] [Online]. Available: [www.robots.ox.ac.uk/~pnewman/TheMOOS/](http://www.robots.ox.ac.uk/~pnewman/TheMOOS/)
- [25] D. Eickstedt and S. Sideleau, "The backseat control architecture for autonomous robotic vehicles: A case study with the Iver2 AUV," *Marine Technology Society Journal*, vol. 44, no. 4, pp. 42–54, Aug. 2010.
- [26] [Online]. Available: [www.moos-ivp.org](http://www.moos-ivp.org)
- [27] [Online]. Available: [gobysoft.org](http://gobysoft.org)